Emergence and spread of outbreak-adapted *Candidozyma auris* harboring mutations in *RBA1*

Laura A. Doorley[1], Alyssa A. La Bella[2], Sarah J. Jones[1], Guolei Zhao[3], Mohammad Asadzadeh[4], Quanita J. Choudhury[1], Suhail Ahmad[4], Eiman Mokaddas[4,5], Inaam Al-Obaid[6], Wadha Alfouzan[4,7], Khalifa Al-Banwan[4,8], Teresa O'Meara[3] Felipe H. Santiago Tirado[2], Ana L. Flores Mireles[2], Jeffrey M. Rybak[1*]

[1] Department of Pharmacy and Pharmaceutical Sciences, St. Jude Children's Research Hospital, Memphis, TN 38105, USA.
[2] Department of Biological Sciences, University of Notre Dame, Notre Dame, IN 46556, USA
[3] Department of Microbiology and Immunology, University of Michigan, Ann Arbor, MI 48109, USA.
[4] Department of Microbiology, Faculty of Medicine, Kuwait University, Jabriya 46300, Kuwait.
[5] Department of Microbiology, Ibne-Sina Hospital, Shuwaikh, Kuwait
[6] Department of Microbiology, Al-Sabah Hospital, Shuwaikh, Kuwait
[7] Department of Microbiology, Farwaniya Hospital, Farwaniya, Kuwait
[8] Department of Microbiology, Amiri Hospital, Kuwait City, Kuwait

[*]Corresponding author: Jeffrey.Rybak@stjude.org

Jeffrey M. Rybak, PharmD, PhD
Assistant Member
Department of Pharmacy and Pharmaceutical Sciences
St. Jude Children's Research Hospital
262 Danny Thomas Place
Chili's Care Center, I5304, Mail Stop #313
Memphis TN, 38105

Office: 901.595.2368
Fax: 901.595.3125

ABSTRACT

Candidozyma auris (formerly *Candida auris*) is an emerging healthcare-associated fungal pathogen, increasingly isolated from clinical outbreaks of infection, and with a high propensity to colonize and persist on patients and within the medical environment. Here, we leveraged a large collection of *C. auris* isolates from multi-facility clinical outbreaks within the same urban area to identify genomic patho-adaptations that promote persistence and dissemination in the healthcare environment. Genomic and phylogenetic analyses revealed loss-of-function mutations in the uncharacterized *C. auris* transcription factor gene *RBA1* to have independently emerged multiple times within these outbreaks. We provide evidence that loss of *RBA1* results in increased *C. auris* adhesion to plastic and human keratinocytes, enhances biofilm formation in multiple conditions, and exacerbates fungal burden in a mouse model of catheter-associated urinary tract infection. Finally, we uncover that loss-of-function mutations in *RBA1* have independently emerged during multiple outbreaks of *C. auris* infections across the globe, and that *RBA1* mutant lineages are present among isolates collected from large ongoing clinical outbreaks. Taken together, the results of this study reveal loss-of-function mutations in the *C. auris RBA1* as a novel and clinically relevant genetic determinant of enhanced outbreak characteristics and virulence factor-gene expression.

56 **INTRODUCTION**

57 *Candidozyma auris* (formerly *Candida auris*) is an emerging pathogenic yeast first
58 identified in 2009 and later recognized by the World Health Organization as a critical threat to
59 global public health in 2022[1, 2]. Initially isolated from a limited number of individual patient
60 infections, *C. auris* was soon revealed as the cause of multiple nosocomial outbreaks of invasive
61 fungal infections across the globe[3]. Now, *C. auris* outbreaks have been reported from more than
62 50 countries, representing thousands of documented infections annually, including 4,514 cases
63 in 2023 in the United States alone[4, 5, 6]. When appropriately treated, outcomes of *C. auris*
64 infections are similar to those previously associated with invasive candidiasis, with crude mortality
65 rates ranging from 30 to 75%, depending on affected patient population and severity of disease[7,
66 8]. However, timely and effective treatment of *C. auris* infections is often complicated both by
67 challenges in the clinical identification of *C. auris* using conventional techniques, and by high rates
68 of resistance to commonly employed antifungal drugs[3].

69 Further distinguishing *C. auris* from other fungal pathogens, *C. auris* is not known to be
70 ubiquitous within common natural environmental reservoirs nor is it a member of the normal
71 human microbiota[9]. *C. auris* infections are, instead, healthcare-associated and typically occur
72 following a horizontal transfer to vulnerable patients within hospital settings[10]. Multiple studies
73 have demonstrated that once introduced into the medical environment, *C. auris* rapidly spreads
74 among both patients and medical surfaces, acting as an invasive species in these healthcare
75 settings. As a result, clinical *C. auris* infections routinely occur in series or as clustered clinical
76 outbreaks, sometimes spanning multiple facilities or institutions within an affected healthcare
77 network[11, 12]. Further, while *C. auris* isolates exhibiting decreased susceptibility to the polyene and
78 echinocandin classes of antifungals were initially associated with acquisition of resistance-
79 conferring mutations during treatment of individual patients, dissemination of antifungal-resistant
80 and treatment-adapted lineages has now been repeatedly documented[13, 14, 15].

81 As with other healthcare-associated and multi-drug-resistant pathogens, the
82 characterization and tracking of emergent microbial lineages with traits impacting clinical
83 outcomes is paramount to infection prevention and treatment. Prior study of *C. auris* evolution
84 during infection and exposure to clinically relevant stressors has largely focused on the
85 emergence of antifungal resistance[15, 16, 17, 18]. We and others have shown, through both *in vitro*
86 evolution experiments and by studying sets of isogenic clinical isolates, that *C. auris* is capable
87 of rapidly adapting to antifungal-induced stress and that multiple independent drug-resistant
88 lineages can emerge after only a single antifungal exposure[15, 16, 17, 18]. However, investigations of
89 patho-adaptation in the clinical setting or during outbreaks of infections remains unexplored.
90 In this work, we leveraged a collection of 70 *C. auris* clinical isolates from multi-institutional
91 outbreaks of infection to identify novel *C. auris* genetic markers and link them to traits driving
92 persistence and outbreak potential in clinical settings. We identified multiple independent lineages
93 of *C. auris* harboring distinct mutations in a previously uncharacterized fungal transcription factor,
94 here named, Repressor of Biofilm and Adhesion 1 (*RBA1*). Genetic and transcriptomic
95 interrogation revealed loss of *RBA1* to result in enhanced biofilm formation, increased adhesion
96 to multiple surfaces including human keratinocytes, and significantly elevated expression of
97 *C. auris* adhesins and virulence factors. Moreover, loss of *RBA1* was found to significantly
98 increase fungal burden in a mouse model of catheter-associated urinary tract infection (CAUTI),
99 an infection characteristically involving biofilms in urine where *C. auris* is often isolated[19]. Finally,
100 analysis of publicly available whole genome sequencing data revealed numerous distinct *RBA1*
101 mutations present in hundreds of clinical isolates, demonstrating consistent and convergent loss-
102 of-function mutations from isolates from well-documented and ongoing clinical outbreaks of
103 *C. auris* infections across the globe. Collectively these findings demonstrate *RBA1* encodes a
104 repressor of *C. auris* biofilm and adhesion and implicate mutations in *RBA1* as clinically relevant
105 adaptations promoting *C. auris* survival during healthcare-associated outbreaks of infection.
106

107 **RESULTS**

108 **Clinical emergence of multiple *C. auris* outbreak lineages carrying *RBA1* mutations.**

109 WGS analysis revealed all *C. auris* isolates belonged to Clade I, one of three major genetic
110 clades previously linked to healthcare-associated outbreaks[20]. This included 34 and 36 isolates
111 from the previously described subclades Ib and Ic, respectively[21]. A total of 155,135 SNPs were
112 identified among the 70 included isolates as compared to the Clade I reference genome
113 (B8441v3), with 46,231 predicted to impact coding regions. As anticipated from characteristically
114 fluconazole-resistant Clade I isolates, all isolates were found to harbor one or more mutations in
115 the genes *ERG11*, *TAC1B*, and/or *MRR1*, which we and others have previously shown to directly
116 contribute to fluconazole resistance[18, 22, 23, 24]. Additionally, 16 isolates were found to possess
117 mutations known to contribute to echinocandin resistance (altering *FKS1*) and 4 isolates
118 possessed mutations in genes associated with amphotericin B resistance (*ERG3*, 1 isolate;
119 *ERG6*, 3 isolates)[15, 25, 26].

120 Phylogenetic analysis revealed the population structure of this collection to consist of 69
121 isolates grouping into three major clusters, with 35, 24, and 10 isolates grouping into clusters A,
122 B, and C, respectively. The remaining single isolate (SKU043) did not group into a larger cluster
123 and was more distantly related (**Fig. 1**). Within clusters, isolates were found to be largely clonal,
124 with an average of 5.3 to 12.6 coding region SNPs separating each isolate (**Fig. S1**), while
125 SKU043 differed from all other isolates by 43 to 113 coding region SNPs. Clusters A and C each
126 contained isolates originating from multiple healthcare facilities within Kuwait, while cluster B
127 originated entirely from a single tertiary care hospital. Notably, multiple instances were identified
128 where isolates from different patients and even different hospitals were found to be more
129 genetically similar than serial isolates originating from the same patient case, as might be
130 expected in the setting of a clinical outbreak.

131 To investigate potential patho-adaptations occurring during outbreaks of *C. auris*
132 infections, we further evaluated the WGS data to identify genes where mutations were acquired

133 on multiple occasions and/or mutations emerged and persisted among the outbreak population.
134 Intriguingly, this revealed 19 isolates harboring mutations in a previously uncharacterized *C. auris*
135 gene B9J08_03209 (identified as B9J08_002136 in B8441v2 and hereafter named *RBA1*), which
136 is predicted to encode a fungal-specific zinc-cluster transcription factor. Although initially identified
137 as an ortholog of *WOR2* in *C. albicans,* the proteins are not syntenic, with only 22% sequence
138 identity, primarily located in the DNA-binding domain. The 19 isolates with mutations in *RBA1*
139 included representatives from all three major phylogenetic clusters, including all 10 isolates in
140 cluster C, as well as the non-clustered isolate SKU043. Four different mutations in *RBA1* were
141 identified, all considered likely loss-of-function mutations, with three encoding an early stop codon
142 (upstream of the predicted DNA-binding domain) and one altering a highly conserved cysteine
143 residue in the $Zn(II)_2Cys_6$ DNA-binding motif. The early stop codon mutation, $RBA1^{E47*}$, was found
144 to have emerged and persisted among two intensive care unit patients over the course of eight
145 months, these cases and the associated 13 cluster B isolates were further evaluated to identify
146 the potential clinical impact of *RBA1* mutations.
147
148 **Loss of *RBA1* enhances *C. auris* biofilm formation.**
149 A subset of isolates from patient cases 51 and 53 have been previously characterized with
150 consideration to antifungal susceptibility while investigating the emergence of echinocandin and
151 amphotericin B resistance-conferring mutations, respectively[15, 27, 28]. In brief, patient 51 was a 54-
152 year-old male with a past medical history significant for multiple myeloma admitted to the intensive
153 care unit (ICU) of Hospital F, a tertiary care center associated with Kuwait Cancer Control Center
154 in Kuwait which cares for immunocompromised patients including cancer patients, burn patients
155 and transplant recipients diagnosed and requiring treatment for infectious diseases. Patient 51
156 was receiving a 14-day course of empiric caspofungin treatment when *C. auris* isolate SKU013
157 ($RBA1^{WT}$; wildtype-*RBA1*) was first identified from a culture of their endotracheal tube and
158 considered to represent colonization (**Fig. 2a**). Four successive isolates (**Table 1**) were identified

159 from endotracheal tube cultures, and the presence of respiratory symptoms prompted a 21-day
160 course of empiric caspofungin treatment. During this treatment, isolate SKU018 (*RBA1*^{E47*}) was
161 obtained from the patient's urinary catheter. SKU018 notably exhibited *in vitro* resistance to
162 echinocandins (*FKS1*^{S639F}), although it was still thought to represent likely colonization. SKU020
163 was obtained from a blood culture the day before patient 51 expired. SKU020 also exhibited
164 elevated *in vitro* echinocandin resistance and differed from the earlier respiratory tract isolates
165 SKU016 and SKU017 by only one coding region SNP (*FKS1*^{R1354H}), indicating likely dissemination
166 from the respiratory tract.

167 Patient 53 was a 33-year-old female in the ICU of the same tertiary care hospital (Hospital
168 F) with a significant past medical history for Hodgkin's lymphoma and advanced stage nodular
169 sclerosis. Approximately one month after receiving a 21-day empiric course of liposomal
170 amphotericin B (AmB) for suspected respiratory infection, the patient's respiratory condition
171 worsened and *C. auris* (SKU022) was isolated from the patient's endotracheal tube. Notably,
172 isolate SKU022 harbored the same *RBA1*^{E47*} mutation present in the isolate previously cultured
173 from the urine of patient 51 (SKU018), and genetically these two isolates differed by four coding
174 region SNPs, suggestive of pathogen lateral transmission. Following completion of a 14-day
175 course of caspofungin treatment, two subsequent *C. auris* isolates (both *RBA1*^{E47*}) were cultured
176 from endotracheal tube and tracheal aspirate cultures, prompting a second 14-day course of
177 liposomal AmB. After this second course of AmB, all cultures from respiratory sources remained
178 negative. However, one month later the patient was suspected to have developed a CAUTI and
179 urine cultures yielded isolate SKU031 (*RBA1*^{E47*}). A second 14-day course of caspofungin was
180 initiated after SKU031 was found to be AmB-resistant. Subsequently, AmB-susceptible *C. auris*
181 (SKU032) was cultured from the patient's urine and a third course of liposomal AmB was given.
182 During this third course of AmB, two additional isolates were obtained from urine cultures,
183 SKU033 (*RBA1*^{E47*}) and SKU035 (*RBA1*^{E47*}), and exhibited decreased susceptibility to AmB and

184 echinocandins, respectively. Patient 53 was then transferred to another care facility, precluding
185 further follow-up.

186 Of the 14 isolates cultured from patient 51 and patient 53, 13 were found to be closely
187 related (separated by 2 to 8 SNPs within coding regions, **Fig. S1**) and grouped into cluster B.
188 Seven of these isolates, starting with SKU018 and including all but one isolate later cultured from
189 patient 53, encoded the early stop codon mutation in *RBA1.* While there was no association
190 between antifungal susceptibility and *RBA1* genotype, all seven *RBA1* mutant isolates were
191 observed to exhibit increased biofilm formation under standard laboratory conditions (**Fig. 2b**). As
192 the earliest isolate where the *RBA1*^{E47*} mutation was identified (SKU018) originated from culturing
193 the urinary tract of patient 51, and multiple subsequent isolates with this mutation were isolated
194 from the urinary tract of patient 53, we next used our fibrinogen-urine biofilm model [29] that utilizes
195 serum-supplemented urine and fibrinogen-coated surfaces to evaluate biofilm formation in
196 conditions mimicking the bladder during CAUTI. In this model, isolates carrying the *RBA1*^{E47*}
197 mutation exhibited enhanced biofilm formation as compared to the earliest isolate SKU013
198 (approximately 2 to 6-fold higher), while biofilm formation was relatively unchanged among closely
199 related *RBA1*^{WT} isolates (**Fig. 2c**). To evaluate if other clinically emergent predicted loss-of-
200 function mutations in *RBA1* had a similar effect on biofilm formation, we also compared the biofilm
201 formation of isolates harboring the *RBA1*^{Q174*} (SKU055), *RBA1*^{Q225*} (SKU043), and *RBA1*^{C303S}
202 (SKU056) mutations to their closest available genetic relatives (SKU021, SKU034, and SKU037,
203 respectively) using the same model. In each case, biofilm formation was observed to be
204 significantly higher in the isolates harboring mutations in *RBA1* (**Fig. 2d**), further bolstering the
205 connection between loss of *RBA1* and biofilm formation.

206 As we observed a strong association between *RBA1* genotype and biofilm formation, we
207 hypothesized that loss-of-function mutations in *RBA1* are a genetic determinant of enhanced
208 *C. auris* biofilm formation. To test this hypothesis, we next generated the *RBA1*-knockout (*Δrba1*)
209 and *RBA1*-revertant (*Δrba1*::*RBA1*$^{+}$) control strains in the SKU013 clinical isolate background and

210 evaluated biofilm formation. In the fibrinogen-urine model, *Δrba1* strains were found to exhibit
211 significantly increased biofilm formation (3.9 to 4.8-fold greater than SKU013; $p<0.0001$). This
212 enhancement of biofilm formation resembled the isogenic clinical isolate SKU018 which carries
213 the *RBA1*^{E47*} mutation (3.3-fold greater than SKU013; $p<0.0001$) (**Fig. 3a**). Importantly,
214 restoration of the *RBA1* gene in *Δrba1*::*RBA1*$^{+}$ control strains returned biofilm formation to levels
215 comparable to SKU013.

216 We further investigated the impact of *RBA1* using a plasma-RPMI biofilm model that
217 utilized serum-supplemented RPMI culture media and human plasma-coated surfaces to evaluate
218 biofilm production that could apply more generally to clinical settings. Once again, *Δrba1* strains
219 were found to produce more robust biofilms (6.2 to 6.8-fold greater than SKU013; $p<0.0001$),
220 while *Δrba1*::*RBA1*$^{+}$ control strains closely matched the biofilm formation of SKU013 (**Fig. 3b**).
221 Examination of the plasma-RPMI biofilms using scanning electron microscopy, showed scattered
222 patches of biofilm predominantly consisting of one to two layers of cells for both SKU013 and
223 *Δrba1*::*RBA1*$^{+}$ (**Fig. 4a**). By comparison, *Δrba1* strains formed more confluent biofilms of variable
224 but generally greater thickness with greater production of extracellular matrix. (**Fig. 4b**).
225

226 **Loss of *RBA1* increases expression of *C. auris* adhesins and virulence factors.**

227 As *RBA1* is predicted to encode a transcription factor and our earlier experiments had
228 shown loss of *RBA1* significantly enhances biofilm formation, we next evaluated the impact of
229 *RBA1* on the *C. auris* transcriptome during both planktonic and biofilm growth conditions using
230 our *Δrba1* strain and the parental *RBA1*^{WT} isolate SKU013. When cells were grown to exponential
231 growth phase in RPMI tissue culture media under planktonic conditions, transcriptional profiling
232 by RNAseq revealed loss of *RBA1* to have a modest impact, and only 55 of 5,594 *C. auris* genes
233 (0.98%) were differentially expressed (≥|1.5| fold-change and false discovery rate [FDR] ≤0.05)
234 (**Fig. 5a**). Of these, 42 genes were upregulated in the absence of *RBA1*, and these genes were

235 enriched for those involved in biofilm formation (p= 1.60e-07) and cell aggregation (p= 2.18e-07),
236 and no enrichment for biological processes was found among the 13 down-regulated genes. By
237 comparison, when cells were harvested from actively growing biofilms, 701 of 5,594 genes
238 (12.53%) were observed to be differentially expressed, including 250 and 451 genes which were
239 up- and down-regulated in the *Δrba1* strain, respectively (**Fig.5b**). Up-regulated genes were
240 enriched for those involved in transmembrane transport (p= 0.01351), regulation of RNA
241 biosynthetic process (p=0.02583), cell aggregation (p=0.05187), and regulation of primary
242 metabolic process (p=0.07722), while down regulated genes were enriched for 18 different
243 biological processes including protein biosynthetic process (p= 2.35e-28), macromolecule
244 biosynthetic process (p= 4.05e-10), premeiotic DNA replication (p= 0.00273), and steroid
245 biosynthetic process (p= 0.02579). Thirty-two *C. auris* genes were up-regulated in the absence
246 of *RBA1* under both growth conditions, and these genes were enriched for those involved in
247 biofilm formation and cell aggregation (**Fig. 5c**). Notably, this included four *C. auris* adhesins
248 (*ALS4112/ALS5, IFF4*, *IFF4109*, and *SCF1*), three of which we have previously shown to impact
249 virulence in a mouse model of invasive candidiasis[30, 31].

250 As many genes in the *C. auris* genome remain uncharacterized and/or currently have
251 incomplete annotations, we further evaluated differential expression among *C. auris* genes with
252 homology to those associated with adhesion, biofilm formation, and cell wall architecture in the
253 model pathogenic yeast *Candida albicans.* This revealed four additional *C. auris*-specific adhesins
254 (B9J08_004110, B9J08_004451, B9J08_004195, and *HYR3*), six additional cell wall-associated
255 proteins (B9J08_002109, B9J08_005545, B9J08_003550, *HGC1*, *PHR1*, and *XOG1*), seven
256 GPI-anchored proteins (B9J08_000892, B9J08_001409, B9J08_00116, B9J08_000438,
257 B9J08_003591, B9J08_00560, and *PGA52*), and three aspartic-type endopeptidases (*SAP1*,
258 *SAP6*, and *SAP7*) exhibiting differential expression under biofilm conditions in the absence of
259 *RBA1* (**Fig. 5d**). Notably, four of the differentially expressed genes associated with the fungal cell
260 wall, B9J08_002109, B9J08_003350, *PHR1*, and *XOG1*, are the predicted orthologs of

261 *C. albicans* cell wall proteins known to be involved in cell wall remodeling, cell wall masking from
262 immune detection, and response to host immune cells[32, 33, 34]. Finally, as *RBA1* appears to repress
263 biofilm formation in *C. auris,* we also examined the expression of *C. auris* orthologs of genes
264 known to regulate biofilm formation in the model pathogenic yeast, *Candida albicans.* Two and
265 17 of these genes were found to be differentially expressed under planktonic and biofilm
266 conditions, respectively. *UME6* and B9J08_002529 (ortholog of *C. albicans BRG1*), exhibited
267 significantly increased expression in the *Δrba1* strain under planktonic conditions, and in
268 *C. albicans* both of these genes are known to be important positive regulators of hyphal growth
269 and biofilm formation. Further, *UME6* has previously been shown to impact *C. auris* biofilm
270 formation when overexpressed and artificially hyper-activated through HA-tagging of the putative
271 transcription factor activation domain[35]. Under biofilm conditions, 14 genes orthologous to those
272 known to regulate biofilm formation in *C. albicans* were up-regulated, notably including the
273 *C. auris* orthologs of *AHR1*, *EFG1*, *RFG1*, *BCR1*, *BRG1*, and *WOR1*, and 3 genes were down-
274 regulated (orthologs of *C. albicans CRZ2*, *CZF1*, and *ZCF4*). These findings demonstrate that
275 *RBA1* significantly impacts regulation of *C. auris* gene expression during biofilm formation and
276 suggest that *RBA1* may play a central regulatory role in this clinically impactful process.
277

278 **Loss of *RBA1* enhances *C. auris* adhesion to plastics and human keratinocytes**

279 A key clinical characteristic of *C. auris* is its ability to adhere to and persist on a variety of
280 surfaces in the nosocomial environment, including medical equipment and patient skin. As our
281 transcriptional profiling revealed loss of *RBA1* enhanced the expression of an assortment of
282 *C. auris* adhesin-encoding genes, we hypothesized that loss of *RBA1* would enhance *C. auris*
283 adhesion to multiple substrates. To test this, we first evaluated the adherence of our *Δrba1* and
284 *Δrba1*::*RBA1*$^{+}$ strains, as well as the isogenic clinical isolates SKU013 and SKU018, to
285 polystyrene plastic under a variety of conditions. After 90 minutes of exposure in RPMI tissue
286 culture media, SKU018 and the *Δrba1* strains exhibited greater adhesion than SKU013 to both

287 polystyrene and tissue culture-treated polystyrene (**Fig. 6a, b**). This difference was magnified
288 when the polystyrene well plates were pre-treated with human plasma, with or without the addition
289 of 10% human serum to the RPMI culture media (**Fig. 6c, d**). By contrast, *Δrba1*::*RBA1*$^{+}$ control
290 strains phenocopied the parental SKU013 under all conditions.

291 Next, we evaluated whether loss of *RBA1* promotes adhesion of *C. auris* to human
292 keratinocytes. After 60 minutes of exposure, *Δrba1* strains were observed to exhibit enhanced
293 adherence to a confluent culture of human N/TERT keratinocytes, while neither *Δrba1*::*RBA1*$^{+}$
294 controls strains nor SKU018 differed from the SKU013 control (**Fig. 6e, f**). Outbreak isolates
295 harboring the *RBA1*^{Q174*} (SKU055), *RBA1*^{Q225*} (SKU043), and *RBA1*^{C303S} (SKU056) mutations
296 were similarly found to exhibit enhanced adhesion to keratinocytes as compared to their closest
297 available genetic relatives (**Fig. 6g, h**) further supporting the connection between loss of *RBA1*
298 and enhanced adherence to human keratinocytes. Taken together, these results confirm that loss
299 of *RBA1* significantly enhances *C. auris* adhesion characteristics under a variety of conditions.
300

301 **Loss of *RBA1* increases fungal burden during catheter-associated urinary tract infections.**

302 As we had observed that loss of *RBA1* increased *C. auris* adhesion, biofilm formation, and
303 the expression of the previously characterized virulence factors *SCF1*, *IFF4109*, and
304 *ALS4112/ALS5*, we next sought to evaluate the impact of *RBA1* on *C. auris* virulence *in vivo*
305 during a model of biofilm-related infection. To accomplish this, we utilized our mouse model of
306 CAUTI [29, 36], where immunocompetent mice were catheterized and the bladder of each mouse
307 was challenged with *C. auris* transurethrally 24 hours prior to sacrifice for evaluation of fungal
308 burden and systemic dissemination of infection. Importantly, this mimics a clinical scenario where
309 *C. auris* is often cultured from patients with urinary catheters and is relevant to multiple patient
310 populations at increased risk of *C. auris* colonization and infection. In this model, the *Δrba1* strain
311 was found to exhibit a 6.8-fold increase in bladder tissue fungal burden (p= 0.0435) by 24 hours
312 post-infection, as compared to SKU013 (**Fig. 7**). Moreover, a trend toward increased

313 dissemination of the *Δrba1* strain to kidney and spleen tissues was also observed, and one mouse
314 infected with the *Δrba1* strain was found to have detectable fungal burden in cardiac tissue. These
315 findings suggest that loss of *RBA1* may also enhance virulence of *C. auris* during clinical infections
316 such as CAUTI.
317

318 **Mutations in *RBA1* have emerged during numerous *C. auris* clinical outbreaks**

319 Having identified a consistent signature for *RBA1* mutations during documented clinical
320 outbreaks of *C. auris* infections in Kuwait and after demonstrating that these mutations confer
321 phenotypes advantageous to *C. auris* persistence, we hypothesized that *RBA1* mutations have
322 also likely occurred during *C. auris* outbreaks in other countries as well. To test this, we leveraged
323 publicly available *C. auris* WGS data collected for infection control and outbreak tracking to
324 identify mutations in the *RBA1* gene. WGS data are freely available for 2181 *C. auris* clinical
325 isolates. A total of 94 mutations in *RBA1* were identified, and a total of 310 isolates were found to
326 carry one or more of the 58 identified non-synonymous or nonsense *RBA1* mutations, including
327 representatives of the *C. auris* major genetic clades I, II, and IV. The majority of the identified non-
328 synonymous/nonsense mutations are considered as likely loss-of-function mutations (40; 61.5%),
329 resulting in early stop codons, frameshift mutations, or alterations within the highly conserved
330 DNA-binding domain (**Fig. 8a**), similar to the mutations we initially identified from the Kuwait
331 outbreak collection. We next evaluated meta data and associated publications characterizing
332 identified isolates harboring non-synonymous *RBA1* mutations to determine those which could be
333 definitively tied to documented outbreaks of infection. This revealed 10 *RBA1* mutations from
334 documented outbreaks of *C. auris* infection which occurred on four continents and were caused
335 by isolates representing both genetic clades I and IV (**Fig. 8b**) [12, 20, 37, 38, 39, 40]. Notably, this included
336 two instances where *RBA1* mutations arose during Indian outbreaks[41] initially reported in 2013,
337 one of the earliest reported outbreaks in South America[37] where three distinct *RBA1* mutant
338 linages emerged, as well as two instances of *RBA1* mutations occurring during ongoing outbreaks

339 in the United States[38, 42]. These findings clearly demonstrate mutations in *RBA1* have previously
340 occurred during a multitude of *C. auris* outbreaks, and further suggest that these mutations confer
341 a competitive advantage to *C. auris* in the healthcare environment.
342
343 **DISCUSSION**
344 Unique among fungal pathogens, *C. auris* poses challenges to clinicians reminiscent of
345 healthcare-associated bacterial pathogens such as *Acinetobacter baumannii* and *Enterococcus*
346 *faecium*, frequently being associated with clinical outbreaks of infection and multi-drug
347 resistance[3, 10]. Unlike other agents of invasive candidiasis, *C. auris* is not considered as part of
348 the human normal flora and is not known to be widely distributed in environmental reservoirs.
349 Instead, *C. auris* infections are currently thought to be acquired predominantly through
350 dissemination of recently emergent drug-resistant, and possibly infection-adapted, lineages within
351 medical environments, leading to the infection of vulnerable patient populations[3, 20]. Thus, as with
352 other healthcare-associated pathogens, the identification of *C. auris* evolution during clinical
353 outbreaks and characterization of traits promoting the persistence among human patients is
354 essential to both preventing infections and mitigating prolonged outbreaks of infection.
355 Previous studies of isolates from infection outbreaks have largely focused on poor clinical
356 or microbiologic outcomes driven by mutations leading to antifungal resistance[15, 17, 18, 25, 27, 43, 44].
357 Here, we analyzed samples from outbreaks in Kuwait to identify genomic and microbiological
358 elements which may promote transmission and persistence of *C. auris* in clinical settings. Rather
359 than distinct clustering of serial isolates from individual patient cases, phylogenetic analysis
360 identified isolate clusters originating from multiple patients indicating multiple instances of
361 pathogen lateral transmission consistent with clinical dissemination. Interestingly, while numerous
362 cases of isolates acquiring mutations associated with echinocandin and AmB resistance were
363 identified, persistence and spread of these multi-drug-resistant lineages was not observed in this
364 study. Conversely, among both phylogenetic clusters B and C, closely related isolates harboring

365 acquired *RBA1* mutations were cultured from multiple patients over periods of time spanning
366 many months. While there was no association between antifungal susceptibility and *RBA1*
367 genotype, *C. auris* isolates carrying clinically acquired loss-of-function mutations in *RBA1* were
368 observed to exhibit enhanced biofilm formation as compared to those with wildtype *RBA1*
369 sequences.

370 Biofilms are critically important to human public health as they promote microbial survival
371 in a variety of environments, demonstrating increased resilience to disinfectants and
372 antimicrobials, and contribute to pathogen dissemination and the establishment of new infections.
373 In fact, the majority of human infections involve biofilms either within human tissues or on the
374 surface of in-dwelling medical devices such as catheters or prosthetic implants [45]. As numerous
375 clinical isolates from the studied clinical outbreaks in Kuwait were isolated from the urine of
376 catheterized patients or the respiratory secretions of patients with endotracheal tubes, we
377 hypothesized that the identified loss-of-function mutations in *C. auris RBA1* represented a
378 clinically emergent adaptation promoting pathogen success in the medical environment through
379 enhanced biofilm formation. Genetic interrogation of the impact of *C. auris RBA1* definitively
380 demonstrated loss of this gene enhanced biofilm formation when evaluated using *in vitro* models
381 mimicking clinically relevant conditions including those specific to CAUTI, an infection from where
382 *C. auris* is frequently isolated. Microscopic evaluation revealed biofilms formed by *Δrba1* strain to
383 be thicker, more confluent, and to include more extracellular matrix on the biofilm surface. This
384 enhancement of biofilm formation may represent a selective pressure which promoted the
385 emergence and persistence of *RBA1* mutant lineages during the studied clinical outbreaks.

386 Subsequent characterization of the impact of *RBA1* on gene expression by transcriptional
387 profiling revealed a narrow role in *C. auris* cells growing under planktonic conditions, and a much
388 wider influence on gene expression when cells were grown in biofilms. Under both conditions,
389 however, *Δrba1* strains exhibited increased expression of a multitude of cell surface adhesins,
390 including multiple genes we have previously shown to significantly impact *C. auris* virulence

391 during infection. The two previously characterized *C. auris*-specific adhesins, *SCF1* and
392 *ALS4112/ALS5,* were substantially elevated in the *Δrba1* strain grown in planktonic conditions,
393 with both genes exceeding a 7-$\log_2$-fold increase over the SKU013 parental control. As these
394 adhesins are known to be critical to the ability of *C. auris* to adhere to a variety of substrates
395 including human skin[30, 31], this suggested that *RBA1* may impact the propensity of *C. auris* to both
396 colonize patients and establish new biofilms. Further investigation of gene expression in biofilms
397 demonstrated that a wide variety of genes predicted to encode *C. auris* cell surface proteins, cell
398 wall constituents, secreted enzymes, and transcriptional regulators were differentially expressed
399 in the *Δrba1* strain. Intriguingly, this also included the *C. auris* orthologs of *C. albicans ENG1* and
400 *YWP1*, two secreted beta-glucanases which are known to play critical roles in cell wall beta-
401 glucan masking[32, 33, 34]. This finding, combined with the altered expression of a multitude of GPI-
402 anchored cell surface proteins and the differences in extracellular matrix production observed by
403 scanning electron microscopy, suggests that the loss of *RBA1* may also facilitate evasion of
404 *C. auris* detection from host defenses during infection.

405 Following the identification of dramatically increased expression of *C. auris* adhesins
406 *SCF1* and *ALS4112/ALS5* in the *Δrba1* strain under planktonic growth conditions, we next
407 examined whether loss of *RBA1* would impact the ability of *C. auris* to adhere to surfaces where
408 we have previously shown *SCF1* and *ALS4112/ALS5* to play a significant role[30, 31]. Strains lacking
409 *RBA1* were found to exhibit enhanced adhesion to human keratinocytes as well as polystyrene
410 surfaces both with and without human plasma treatment, which mimics the deposition of host
411 factors such as fibrinogen on medical device surfaces. Moreover, evaluation of three *C. auris*
412 clinical isolates from the Kuwait outbreaks harboring three additional loss-of-function mutations,
413 as compared to their respective closest available genetic relative with a *RBA1*^{WT} allele, again
414 demonstrated loss of *RBA1* to increase adhesion of *C. auris* to human keratinocyte. This finding
415 is of substantial clinical relevance, as it supports that loss of *RBA1* can promote the dissemination
416 of *C. auris* and colonization of patients during a clinical outbreak. Further, patients colonized with

417 *C. auris* strains harboring *RBA1* loss-of-function mutations may pose a greater risk of
418 transmission within the hospital environment.

419 We also examined the impact of *RBA1 in vivo* using a murine CAUTI model which
420 replicates a biofilm-related infection of a site where *C. auris* is commonly isolated. Contrary to
421 other commonly utilized models of pathogenic yeast infection, this model uses mice that have not
422 been immunosuppressed. Instead, immunocompetent mice are made vulnerable to *C. auris*
423 infection through the implantation of a silicone catheter, similar to urinary catheters commonly
424 used among human patients. In this model, the *Δrba1* strain was found to develop a significantly
425 greater fungal burden in the mouse bladder, and a trend towards greater dissemination of the
426 *Δrba1* strain from the urinary tract to other tissues including the heart was observed. These
427 findings further suggest loss of *RBA1* is advantageous during *C. auris* clinical infection. This is
428 clinically significant as CAUTIs often lead to urosepsis with a ~30% 7-day mortality rate [19, 46].
429 Since the urinary tract is a source of ~25% of the all the sepsis cases, patients infected with
430 *C. auris* strains harboring *RBA1* mutation may be predisposed to severe clinical complication.

431 Finally, leveraging the growing body of publicly available WGS data generated through
432 ongoing *C. auris* infection control and prevention efforts, we were able to investigate whether
433 mutations in *RBA1* have emerged during clinical outbreaks in other countries. This approach
434 uncovered dozens of distinct *RBA1* mutations, impacting hundreds of clinical isolates and more
435 than 10% of evaluable samples. *RBA1* mutations were identified among isolates representing
436 three of the major genetic subgroups of *C. auris,* but were notably absent among isolates from
437 clade III*,* suggesting either clade-specific impacts of *RBA1* mutations or a potential bias within
438 samples currently available in the public data set. Like the four *RBA1* mutations identified from
439 the Kuwait outbreaks, the mutations identified from the global collection were predominantly
440 predicted loss-of-function mutations such as those encoding early stop codons, frameshift
441 mutations, or altering highly conserved residues in the zinc-cluster transcription factor DNA-
442 binding domain. Identified isolates with *RBA1* mutations were found to date back to some of the

443 earliest documented clinical outbreaks of *C. auris*, including those in India, England, and
444 Columbia. Additionally, isolates from outbreak lineages actively disseminating in the United States
445 were also found to harbor *RBA1* mutations. Taken together, these findings clearly demonstrate
446 that mutations in *RBA1* have emerged repeatedly during clinical outbreaks of *C. auris* infection
447 and strongly support the notion that the enhancement in adhesion and biofilm formation conferred
448 by these mutations provided a competitive advantage within the medical environment in
449 numerous previous outbreaks.

450 In conclusion, these results call attention to the capacity of *C. auris* to evolve and enhance
451 traits beyond drug resistance during outbreaks of infection by highlighting the unique nature of
452 *C. auris* among other fungal pathogens and identifying mutations in *RBA1* as a potential indicator
453 of outbreak-adapted lineages. As traits conferred by *RBA1* mutations are advantageous to
454 *C. auris* spread and persistence, and as we have identified numerous instances where these
455 mutations have arisen during global outbreaks of infection, the identification and tracking of
456 lineages carrying *RBA1* mutations may be merited as part of infection prevention efforts.
457

458 **MATERIALS AND METHODS**

459 **Ethics Statement**

460 *C. auris* isolates were cultured from various clinical specimens of hospitalized patients in Kuwait.
461 The need for informed consent was waived by the Health Sciences Center Ethics Committee
462 (Approval letter Ref: VDR/EC/3724 dated January 31, 2021) as the clinical specimens were
463 collected as part of routine diagnostic work-up for the isolation of bacterial/fungal pathogens for
464 suspected infections. The results are reported here on deidentified samples without revealing
465 patient identity. All animal care was consistent with the Guide for the Care and Use of Laboratory
466 Animals from the National Research Council. The University of Notre Dame Institutional Animal
467 Care and Use Committee approved all mouse infections and procedures as part of protocol
468 number 25-01-9009. For urine collection, all donors signed an informed consent form, and
469 protocols were approved by the Institutional Review Board of the University of Notre Dame under
470 study #19-04-5273.

471

472 ***C. auris* Isolates**

473 Seventy *C. auris* isolates from previously described multi-institution outbreaks of *C. auris*
474 infections in Kuwait, were obtained by the Mycology Reference Laboratory Department of
475 Microbiology, Kuwait University, Kuwait [47]. All isolates (including names used in publication of
476 their original description) and strains used in this study are listed in **Table S1**. All *C. auris* strains
477 were stored in 40% glycerol stocks at -80°C and cultured at 35°C in liquid YPD (1% yeast extract,
478 2% peptone, 2% glucose) media before plating on Sabouraud dextrose (SD) agar (BD Difco)
479 media to ensure standardized growth for phenotypic testing.

480

481 **Plasmid and strain construction**

482 EPIC-mediated gene editing was used to generate *RBA1* (B8441v3: B9J08_03209)
483 modifications in *C. auris* clinical isolate SKU013 (also known as Kw1432/17). Duplexed guide

484 oligos (Integrated DNA Technologies) (**Table S2**) targeting disruption or reversion of
485 B9J08_03209 were added to the pJMR19 vector using restriction enzyme cloning[26]. Plasmids
486 were maintained in *E. coli* DH5α cells cultured in Luria-Bertani broth supplemented with 5mg/L
487 ampicillin and isolated using QIAprep® Spin Minipreps (Qiagen). Repair templates for *RBA1*-
488 disruption and reversion were amplified from a gBlock sequence (Integrated DNA Technologies)
489 and SKU013 gDNA, respectively, via PCR and purified with QIAquick PCR Purification Kit
490 (Qiagen). All oligos, plasmids, and gBlocks used in this study are listed in **Table S2.** *C. auris*
491 Lithium acetate transformations were then performed as previously described [26] with positive
492 selection on 200µg/mL nourseothricin-supplemented YPD agar. *RBA1* editing was confirmed by
493 both Sanger sequencing at the Hartwell Center at St. Jude Children's Research Hospital (SJCRH)
494 and with long read nanopore sequencing by Plasmidsaurus.
495
496 **Whole genome sequencing**
497 Genomic DNA (gDNA) was extracted from 1mL of overnight liquid YPD cultures using
498 MasterPure™ Yeast DNA Purification kits (Biosearch Technologies) according to manufacturer
499 instructions. Sample libraries were prepared from gDNA by the Hartwell Center (SJCRH) using
500 KAPA HyperPrep (Roche) and sequencing targeting 100x coverage for paired 150bp reads was
501 performed via Illumina NovaSeq. Paired-reads FASTQ files were analyzed using CLC genomics
502 workbench v24.0 (QIAGEN) software. Low quality reads were trimmed with Trim Reads v2.8 and
503 subsequently mapped to the B8441v3 genome (GCA002759435.3) according to CLC-workbench
504 recommendations for match scores, mismatch, insertion, and deletion costs. Local Realignment
505 v2.6 was used to refine unaligned ends and mutations were identified within annotated coding
506 sequences via Fixed Ploidy Variant Detection v2.6 with ploidy=1.
507 Phylogenetic analysis was initiated with Create SNP Tree v1.9 using the Maximum
508 Likelihood Phylogeny v1.4 algorithm. The resulting SNP phylogenetic tree was visualized from
509 Neighbor Joining construction methods specifying Jukes Cantor nucleotide substitution modeling

510 with estimated topology and bootstrapping for 100 replicates. Sequences were deposited in
511 National Center for Biotechnology Information Sequence Read Archive.
512
513 **Biofilm Production Assays**
514 To assess biofilm production in the presence of human plasma, 96-well flat-bottomed
515 plates (VWR, 10861-562) were coated with 100 μL pooled human plasma (Innovative Research
516 Inc, IPLAWBNAC50ML) diluted 1:5 in carbonate-bicarbonate buffer (Sigma C3041-50CAP) and
517 incubated overnight at 4°C. Colonies from overnight SD agar plates were used to generate
518 standardized OD_{600} = 0.5 cell suspensions[48] in RPMI-Biofilm media, consisting of RPMI medium
519 1640 (Gibco) + 3-(4-Morpholino)propane sulfonic acid (MOPS, Fisher Bioreagent) + 2% dextrose,
520 buffered to pH 7 and supplemented with 10% heat-inactivated/male AB human serum (HuS,
521 Sigma-Aldrich). Plasma coatings were gently removed the plates and 200 μL of the cell
522 suspensions were added to the wells and plates were sealed with a breathable (EASYSEAL)
523 membrane. After 90-minutes at 37°C, 250 RPM, plates were gently washed sterile PBS to remove
524 non-adhered cells. Fresh 200 μL of RPMI-Biofilm media was then added back to each well and
525 plates were incubated for 24 hrs at 37°C, 250 RPM. For quantification of biofilm production,
526 supernatants were removed and wells were gently washed twice with PBS. Biofilms were stained
527 with 0.4% crystal violet as previously described[48]. Crystal violet absorbance measured at 595nm
528 on an Agilent BioTek Synergy H1 Microplate Reader. Average media only negative controls were
529 subtracted from the sample reads and values were normalized to SKU013.
530 To replicate biofilm growth replicating the urinary tract environment, 96-well flat-bottomed
531 plates (VWR, 10861-562) were coated with 100 µl of Fg (450 µg/ml) and incubated overnight at
532 4°C.[29] The various strains were grown overnight, shaking in YPD, and the inoculum was
533 normalized to ~1 × 10^6 CFUs/ml. Cultures were then diluted (1:100) into human urine
534 supplemented with 10% heat inactivated human serum and incubated in the wells of the 96-well

535 plate at 37°C for 48 hours. Human urine from at least two healthy female donors between the
536 ages of 20 to 35 were collected and pooled. Donors did not have a history of kidney disease,
537 diabetes, or recent antibiotic treatment. Urine was sterilized with a 0.22-µm filter (VWR 29186-
538 212), pH was normalized to 6.0 to 6.5, and urine was used immediately for the assays. Following
539 biofilm formation, supernatants were removed, and plates were incubated in 200 µl of 0.5% crystal
540 violet for 15 min. Crystal violet stain was removed, and the plate was washed with water to remove
541 the remaining stain. Plates were dried and then incubated with 200 µl of 33% acetic acid for 15
542 min. In another plate, 100 µL of the acetic acid solution was transferred, and absorbance values
543 were measured via a plate spectrophotometer at 595 nm (Molecular Devices SpectraMax ABS).
544 Values were then normalized to SKU013.
545
546 **RNA Extraction**
547 Normalized cell suspensions (OD_{600} = 0.1) from SD replicate platings were diluted ~1:50
548 in 10 mL RPMI-Growth media, prepared from RPMI medium 1640 (Gibco) + MOPS (Fisher
549 Bioreagent) buffered to pH 7 and grown overnight at 35°C, 220 RPM to an OD_{600} = 2.0 ± 0.3.
550 Concentrated cultures were diluted in >20mL RPMI-Growth media to an OD_{600} = 0.2 then split
551 into two 10mL aliquots for direct comparison of planktonic growth and biofilm development.
552 Planktonic cells were grown over 4 hours in 50mL conical at 35°C, 220RPM and pelleted at 4000
553 RPM. For biofilm development cells were transferred to T75 flask pre-coated with 20% human
554 plasma in carbonate-bicarbonate buffer prepared as described above. Following 2 hr incubation
555 at 37°C, non-adhered cells were gently removed and fresh 10mL RPMI-Growth media was added
556 for an additional 4 hr incubation at 37°C. Biofilms were gently washed once with PBS and biofilms
557 were then removed by scraping in the presence of 10mL sterile PBS and pipette transfer to a
558 50mL conical tube for centrifuge pelleting. All pellets were flash frozen in liquid nitrogen and stored

559 at -80°C. RNA was isolated using the Invitrogen RiboPure™ Yeast kit (ThermoFisher Scientific™,
560 USA) per manufacturer's instructions.
561
562 **RNA Sequencing**
563 The Hartwell Center (SJCRH) prepared the RNA libraries using Illumina chemistries per
564 manufacturer's instructions and sequenced the RNA on an Illumina NextSeq (Illumina Inc., USA)
565 using the total stranded RNA-Seq application for paired end runs targeting 150bp reads.
566 Sequenced reads were analyzed with CLC Genomics Workbench version 24.0.1 (QIAGEN).
567 Imported reads were trimmed using default settings for failed reads and adaptor sequences and
568 then subsequently mapped to the *C. auris* B8441 reference genome (GenBank accession:
569 GCA_002759435.3) with paired reads counted as one and expression values set to RPKM.
570 Principal component analysis was utilized for the initial clustering assessment of biological
571 replicates and mismatch, insertion, and deletion costs were set to default parameters for RNA-
572 Seq Analysis 2.7. Differential expression was calculated using negative binomial GLM modeling
573 with whole transcriptome RNA-Seq defaults for normalization with Trimmed Mean of M values,
574 using Differential gene expression v1.4 (CLC genomics workbench, Qiagen). Comparisons were
575 made to the wildtype *SKU013* clinical isolate for each condition. Differential expression was
576 defined as fold changes ≥ 2 or ≤ -2 (FDR p-value ≤0.05)
577
578 **Scanning Electron Microscopy**
579 Sterile silicon chips were loaded into 24-well plate and coated overnight with 0.5mL 20%
580 human plasma in carbonate-bicarbonate buffer. Suspensions of SKU013, *Δrba1*::*RBA1*$^{+}$_a , and
581 Δ*rba1_a* were cultured in RPMI-Biofilm media as described above for biofilm production assays
582 with 0.5mL of cells loaded into the wells. Following 24 hour incubation, wells were gently washed
583 with 1mL PBS and biofilms were fixed with 0.1M sodium cacodylate buffer at pH 7.4 with 0.15%
584 alcian blue, 1% tannic acid, 2.5% glutaraldehyde, 2% paraformaldehyde for 2 hours and stored

585 at 4°C. Preparation, staining, and imaging the fixed biofilms was performed by the Electron
586 Microscopy Division of the Cell and Tissue Imaging Center (CTIC-EM) at SJCRH for SEM Fixed
587 biofilms were washed with 0.1M sodium cacodylate buffer + 0.15% alcian blue prior to osmium
588 tetroxide staining in the presence of 0.15% alcian blue. Imaging was performed on a Zeiss
589 GeminiSEM 460. Scale bars were embedded using ImageJ[49].
590
591 **Polystyrene adhesion assay**
592 Adhesion to flat-bottom 96-well non-tissue culture treated polystyrene plates (CS100-
593 701311, NEST SCIENTIFIC) was assessed in RPMI-Growth+ media, defined as RPMI medium
594 1640 + MOPS + 2% dextrose, buffered to pH 7. Adhesion to tissue culture treated plates
595 (TP92696, TPP Midwest Scientific), was assessed for RPMI-Growth+ media and RPMI-Biofilm
596 media in the presence and absence of human plasma, coated as described above. cells cultured
597 and plates were loaded as described for biofilm production assays. Following a 90-minute
598 incubation at 37°C, 250RPM, wells were gently washed once with PBS to remove non-adhered
599 cells. Adhered cells were stained with 100μL of a 10:1 solution of XTT sodium salt and phenazine
600 methosulfate (VWR International LLC). Absorbances at OD_{492} and OD_{630} were read after 60
601 minutes and values were normalized to SKU013.
602
603 **Keratinocyte adhesion assay**
604 Adhesion of *Candida auris* to human keratinocytes was determined as previously
605 described[30]. Human N/TERT keratinocytes[50] were grown in 96-well plates to complete confluence
606 in keratinocyte-SFM medium (Gibco, 10724-011) supplemented with 30 μg/ml bovine pituitary
607 extract, 0.2 ng/ml epidermal growth factor, and 0.31 mM $CaCl_2$. Overnight *C. auris* cultures were
608 diluted to an OD_{600} of 0.03, and 100 μl of this suspension was added to each well containing
609 keratinocytes. In parallel, an equal volume of culture was added to empty wells, centrifuged (210

610 g, 1 min), and imaged to determine input cell counts, while plates containing keratinocytes were
611 centrifuged under the same conditions and incubated at 37 °C with 5% CO_2 for 1 h. Non-adherent
612 yeast cells were then removed by washing three times with PBS. The remaining cells were fixed
613 in 4% formaldehyde and stained with FITC-conjugated anti-*Candida* antibody (Meridian
614 Bioscience, B65411F; 1:1000). Keratinocyte nuclei and cell bodies were labeled with Hoechst
615 (Thermo Fisher, 62249; 1:1000) and CellMask Deep Red (Thermo Fisher, H32721; 1:5000),
616 respectively.

617 Fluorescent images were acquired at 10X magnification using a BioTek Lionheart FX
618 microscope. The number of adherent *C. auris* cells was quantified using a customized CellProfiler
619 analysis pipeline[30, 51]. Numbers of input cells were determined from brightfield images pre-
620 processed in Fiji/ImageJ (v2.14.0)[49] using a custom macro for edge-based segmentation and
621 binary mask generation. The proportion of adherent to input cells was calculated to assess the
622 adhesion efficiency of each *C. auris* strain.

623

624 **Catheter-Associated Urinary Tract Infection (CAUTI) Modeling**

625 Female C57BL/6 mice (Jackson Laboratory) were subjected to transurethral implantation
626 of a silicone catheter followed by transurethral inoculation of the bladder lumen with ~5×10^5
627 colony forming units (CFU) in PBS, as previously described [36]. Mice were euthanized at 24 hours
628 post-infection by cervical dislocation after anesthesia inhalation and the catheter, bladder,
629 kidneys, spleen, and heart were aseptically harvested. Bladders were weighed and then
630 homogenized for CFUs. The other organs were homogenized, and catheters were cut into small
631 pieces before sonication for fungal CFU enumeration.

632

633 **Statistics and Reproducibility**

634 Statistical parameters and applied analysis methods including exact sample numbers (n)
635 and definitions for representative central value and spread (mean ± SEM, CFU quantifications;

representative modal value (n=3), minimum inhibitory concentrations) are annotated in corresponding figure legends. Data from at least three experiments were pooled for each adhesion and biofilm assay and twice for each *in vivo* mouse assay. One-way ANOVA tests and two-tailed Mann-Whitney *U* tests were performed with GraphPad Prism 10 software (GraphPad Software) for comparisons of described in-vitro assays and in vivo CAUTI experiments, respectively.

For RNA sequencing, statistical analysis was performed using CLC Genomics Workbench version 20.0 (QIAGEN) with paired reads counted as one and expression values set to RPKM. Whole transcriptome differential gene expression analysis was performed with mismatch, insertion, and deletion costs set to default parameters, and a Wald test was used to compare SKU013 against Δ*rba1_a*. Differential expression determined by a fold change of ≥ 2 or ≤ -2 with a False discovery rate (FDR) corrected p value ≤0.05.

ACKNOWLEDGMENTS

This work was supported in part by the St. Jude Children's Research Hospital Children's Infection Defense Center and Center for Infectious Diseases Research awards granted to JMR, by the National Institutes of Health (NIH)/ National Institute of Allergy and Infectious Diseases (NIAID) grant U19-AI181767 awarded to TRP, and by the NIH/ NIAID F32 AI181164 awarded to GZ. This work was supported by institutional funds from the University of Notre Dame (to FHST and ALFM), and by grants from the Good Venture Foundation (Open Philanthropy) (to ALFM), from the National Institutes of Health R01AI177875 and R21AI171742 (to FHST), and R01DK128805 (to ALFM). This research included experiments conducted by the Hartwell Center for Bioinformatics & Biotechnology, the St. Jude Center for Advanced Genome Engineering and the Cell and Tissue Imaging Center - Electron Microscopy (CTIC-EM) which are supported in part by ALSAC and the National Cancer Institute at the National Institutes of Health [P30 CA021765]. The funders had no role in study design, data collection and interpretation, or the decision to submit the work for publication.

AUTHOR CONTIBUTIONS

Conceptualization, J.M.R., T.R.O., F.H.S.T., and A.L.F.M.; methodology, J.M.R., L.A.D., A.A.L., S.J.J., Q.Z., T.R.O., and A.L.F.M.; Investigation, L.A.D., A.A.L., S.J.J., Q.Z., Q.J.C., and J.M.R.; writing—original draft, L.A.D. and J.M.R.; writing—review & editing, L.A.D., A.A.L., S.J.J., G.Z., M.A., Q.J.C., S.A., E.M., I.A., W.A., K.A., T.R.O., F.H.S.T., A.L.F.M., and J.M.R.; funding acquisition J.M.R., T.R.O., F.H.S.T., A.L.F.M., and Q.Z.; supervision, T.R.O., F.H.S.T., A.L.F.M., and J.M.R..

672 **FIGURES AND TABLES**
673

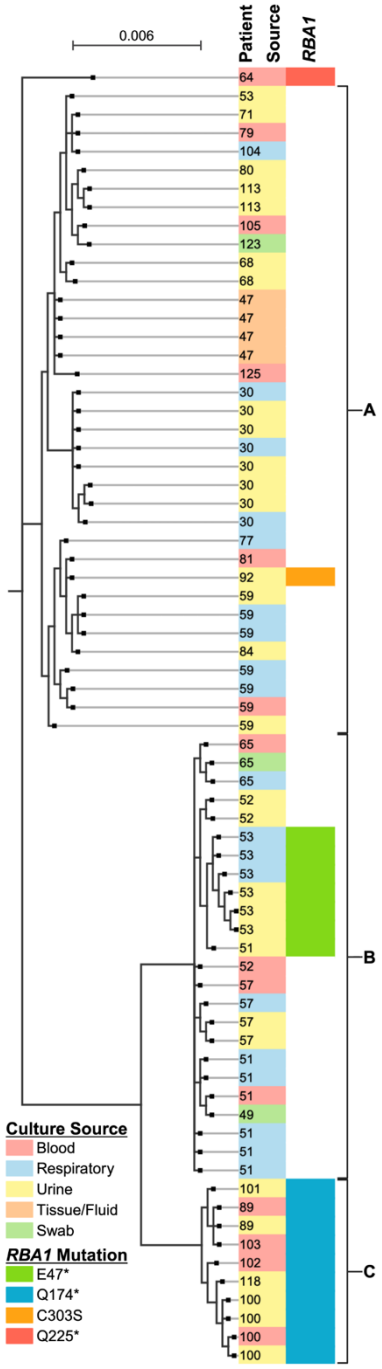

674
675 **Figure 1. Clinical emergence and spread of *C. auris* isolates harboring mutations in *RBA1***
676 **during an outbreak of infections.** Phylogenetic analysis of 70 *C. auris* isolates from a
677 documented outbreak of infections in Kuwait. Branch length termination is indicated with black
678 boxes. Patient case numbers, culture sources, and *RBA1* mutations are indicated on the right.
679

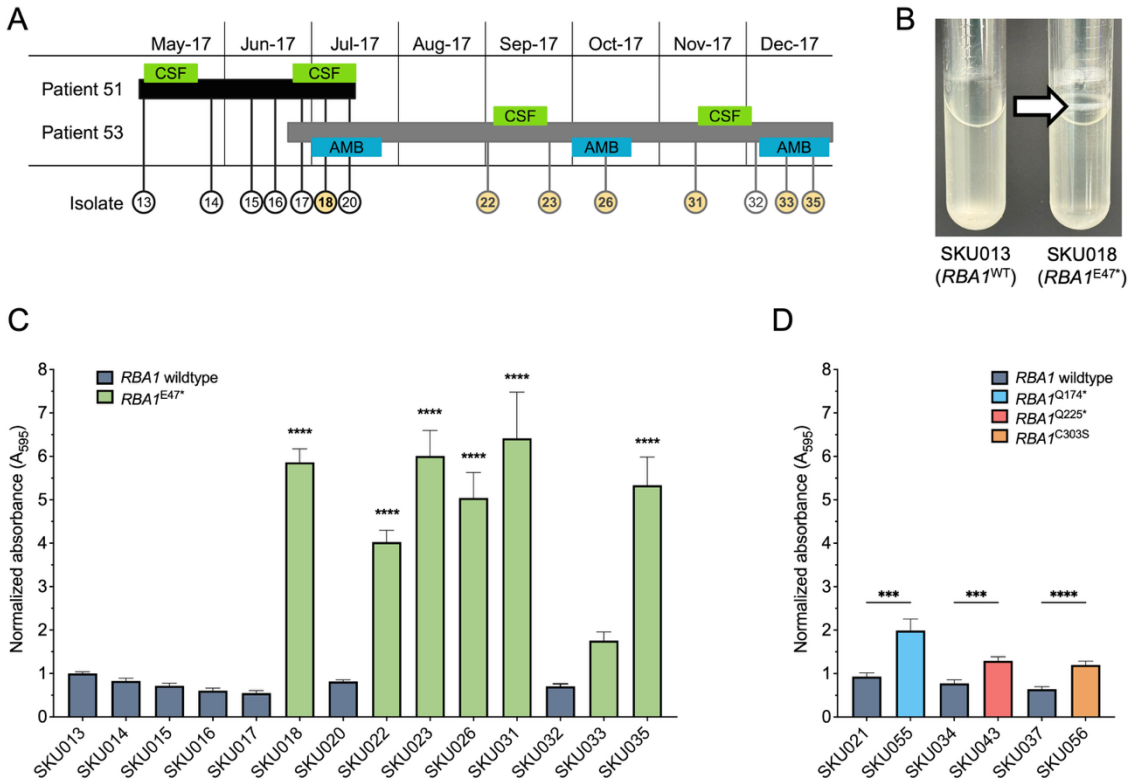

Figure 2. *RBA1* loss-of-function mutations emerge during patient infection and are associated with increased biofilm production A) Timeline of patient cases 51 and 53 with *C. auris* isolation dates and antifungal treatment courses indicated, AMB: liposomal amphotericin B, CSF: caspofungin. Isolate numbers circled with yellow backgrounds indicating *RBA1* mutation. **B)** Visual difference in biofilm formation on sidewall of polystyrene culture tubes after overnight incubation in RPMI media. Arrow indicates visible biofilm ring. **C)** Biofilm production of *C. auris* isolates obtained from patient cases 51 and 53, formed over 48 hours on fibrinogen treated polystyrene in urine supplemented with 10% serum assessed by absorbance at 595 nm wavelength following crystal violet stain and normalized to the initial isolate SKU013. Isolates indicated with dark blue bars have a wildtype *RBA1* allele, while isolates with green bars have the *RBA1*^{E47*} mutation. **D)** Biofilm production of *C. auris* clinical isolates harboring *RBA1*^{Q174*}, *RBA1*^{Q225*}, and *RBA1*^{C303S} mutations and corresponding closest genetic relatives formed over 48 hours on fibrinogen treated polystyrene in urine media supplemented with 10% serum assessed by absorbance at 595 nm wavelength following crystal violet stain and normalized to SKU013. Isolates indicated with dark blue bars have a wildtype *RBA1* allele, while isolates with light blue bars have the *RBA1*^{Q174*} mutation, isolates with red bars have the *RBA1*^{Q225*} mutation, and isolates with orange bars have the *RBA1*^{C303S} mutation.

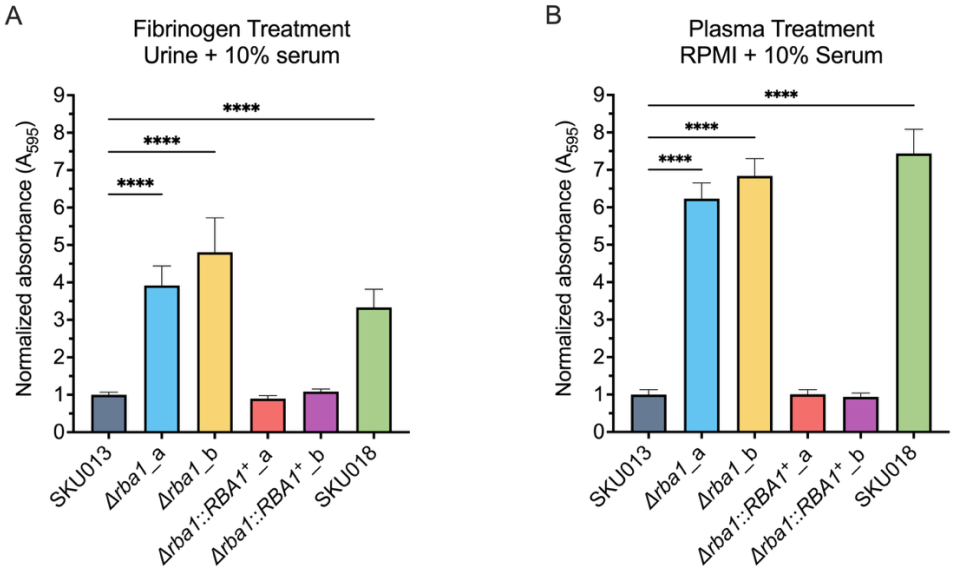

Figure 3. Loss of *RBA1* enhances biofilm production in multiple conditions mimicking difference niche of infection. A) Biofilm production of *C. auris* isolates and *RBA1* strains formed over 48 hours on fibrinogen coated microtiter plates in human urine media supplemented with 10% human serum assessed by absorbance at 595 nm wavelength following crystal violet stain. Absorbance is normalized to SKU013 ($RBA1^{WT}$) with bars representing mean and standard error of the mean. Kruskal-Wallis statistical testing with Dunn's correction for multiple comparisons (GraphPad Prism) showed significant differences between *Δrba1_a, Δrba1_b*, and SKU018 ($RBA1^{E47*}$) when compared to SKU013 ($RBA1^{WT}$) for both adhesion and biofilm production (****P= <0.0001). **B)** Biofilm production of *C. auris* isolates and *RBA1* strains formed over 24 hours on human plasma coated microtiter plates in RPMI tissue culture media supplemented with 10% human serum assessed by absorbance at 595 nm wavelength following crystal violet stain. Absorbance is normalized to SKU013 ($RBA1^{WT}$) with bars representing mean and standard error of the mean. Kruskal-Wallis statistical testing with Dunn's correction for multiple comparisons (GraphPad Prism) showed significant differences between *Δrba1_a, Δrba1_b*, and SKU018 ($RBA1^{E47*}$) when compared to SKU013 ($RBA1^{WT}$) for both adhesion and biofilm production (****P= <0.0001).

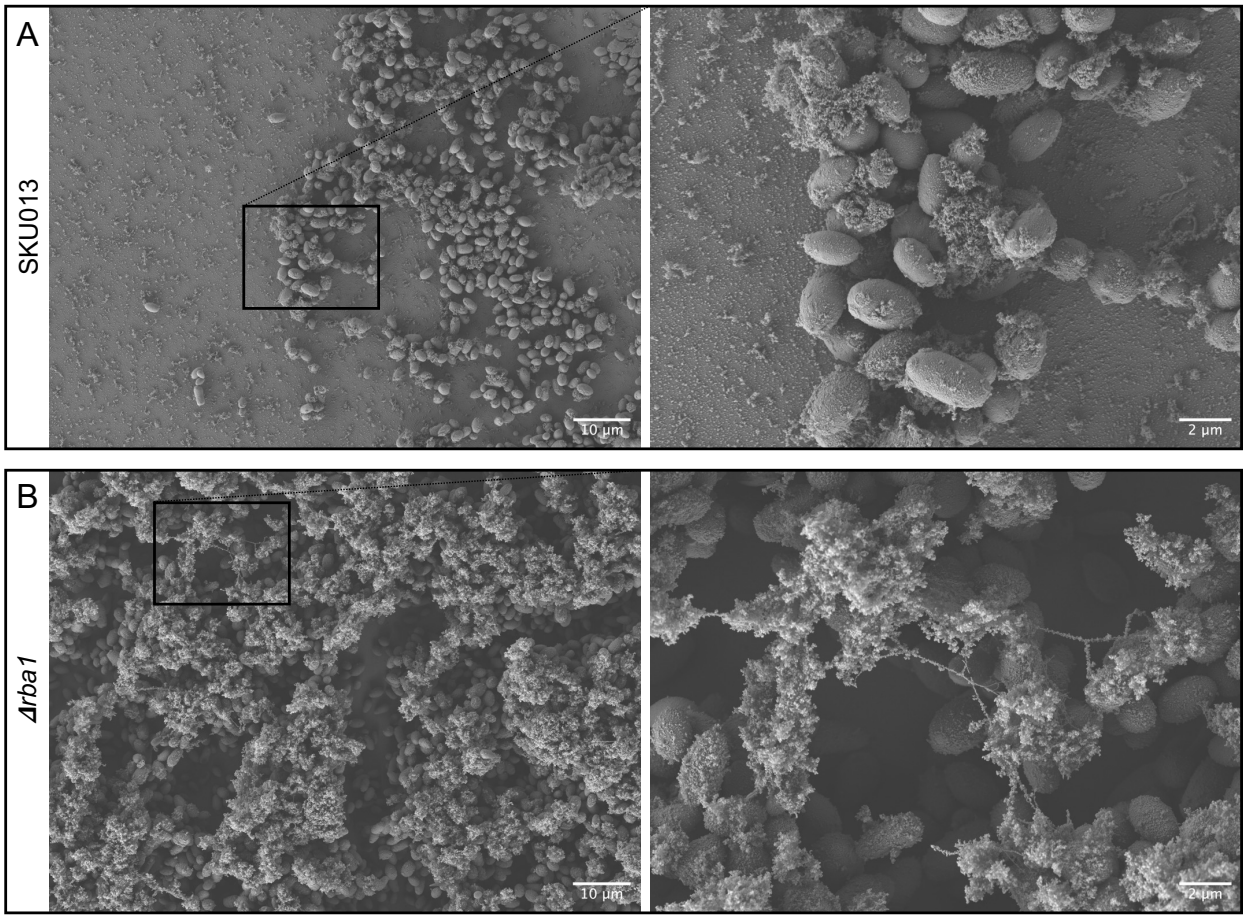

Figure 4. Loss of *RBA1* promotes formation of robust biofilms with greater extracellular matrix. A) Representative SEM images for SKU013 (*RBA1*^{WT}) biofilms formed over 24 hours in RPMI media supplemented with 10% human serum following substrate treatment with human plasma using the 'Silicone substrate–confocal microscopy" method. Black box in left panel indicates area enlarged in right panel. **B)** Representative SEM images for *Δrba1* biofilms formed over 24 hours in RPMI media supplemented with 10% human serum following substrate treatment with human plasma using the 'Silicone substrate–confocal microscopy" method. Black box in left panel indicates area enlarged in right panel.

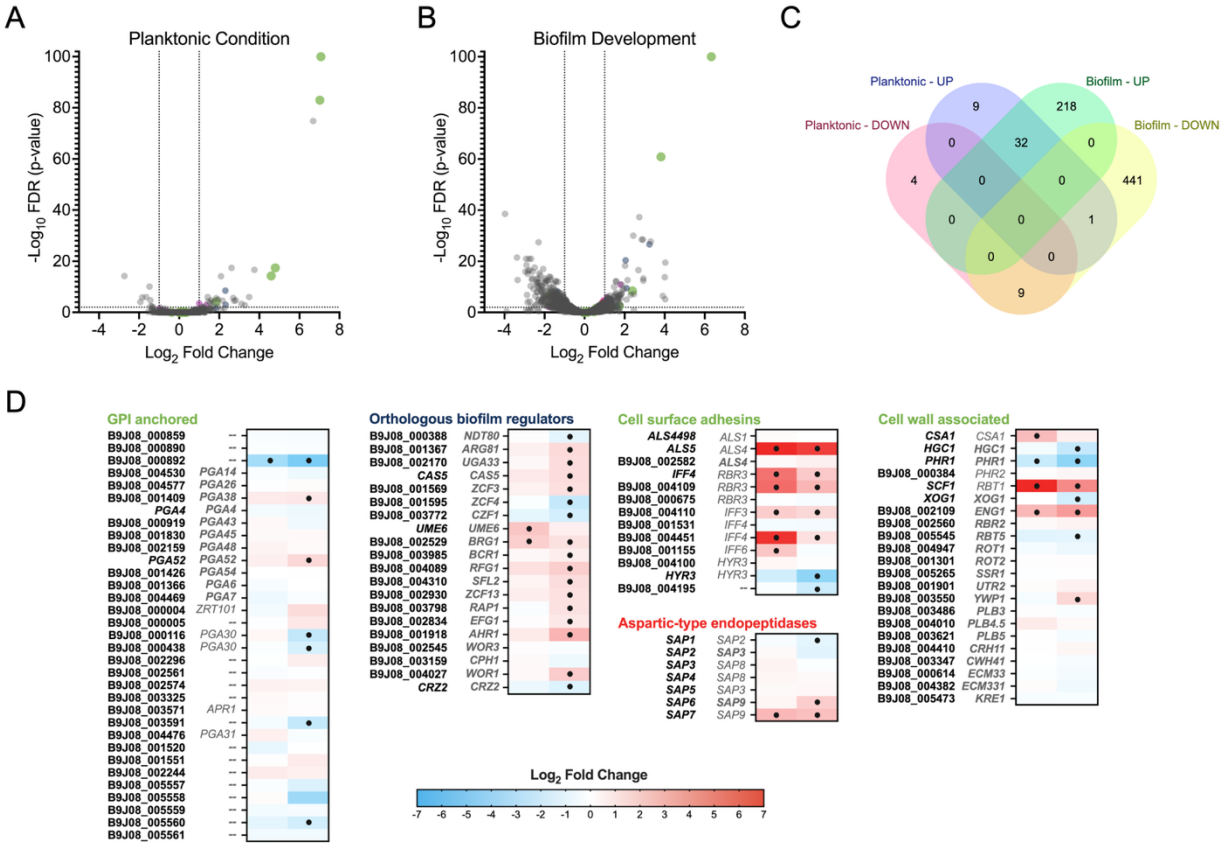

Figure 5. Loss of *RBA1* increases expression of *C. auris* adhesins and virulence factors under both planktonic and biofilm conditions. Volcano plot of differentially expressed genes between clinical isolate SKU013 and *Δrba1* strain during exponential growth phase when cultured under **A)** planktonic growth conditions (10mL RPMI media in 50mL conical tube incubated at 35°C with 220RPM) and **B)** biofilm-forming conditions (10mL RPMI media in plasma-treated T75 flasks for static incubation at 37°C). Genes involved in cell aggregation, biofilm formation, or drug resistance are highlighted in blue, green, and purple, respectively. Dotted lines represent lower limit equivalents for fold changes of ≥1.5 or ≤-1.5 on the x-axis, and a false discovery rate (FDR) p-value ≤0.05 on the y-axis. **C)** Venn diagram comparing differentially expressed genes (≥1.5 or ≤-1.5 on the x-axis, and a false discovery rate p-value ≤0.05) exhibiting up-regulation or down-regulation in the *Δrba1* strain under planktonic or biofilm growth conditions. **D)** Differential expression of *C. auris* gene predicted to encode GPI-anchored proteins, cell surface adhesions, proteins associated with fungal cell wall, aspartic-type endopeptidases, and transcriptional regulators predicted to be orthologous to those known to to be involved in biofilm formation in *Candida albicans*. Similar *C. albicans* genes are listed in gray and are shown in **bold** if predicted to be orthologous. Genes which are differentially expressed (≥1.5 or ≤-1.5 on the x-axis, and a false discovery rate p-value ≤0.05) are indicated with a black dot.

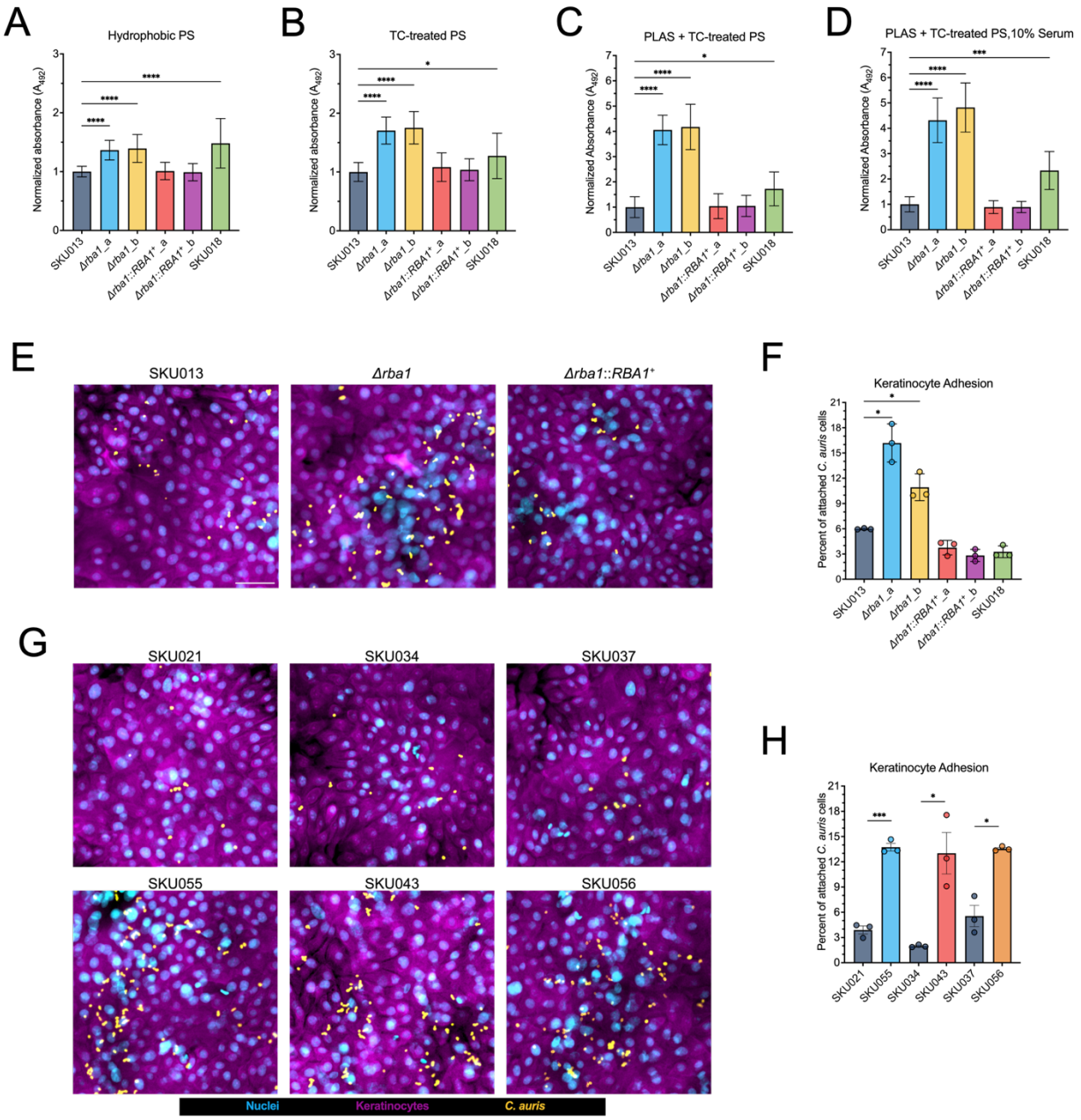

Figure 6. Loss of *RBA1* increases adhesion to both environmental surfaces and keratinocytes. Adhesion of *C. auris* isolates and *RBA1* strains to **A)** untreated polystyrene, **B)** tissue culture treated polystyrene, **C)** human plasma-coated tissue culture-treated polystyrene, and **D)** human plasma-coated tissue culture-treated polystyrene with 10% human serum supplement in RPMI base media after 90 minutes assessed by absorbance at 490 nm wavelength following XTT treatment. **E)** Representative immunofluorescence images showing adherence of SKU013 (*RBA1*^{WT}), *Δrba1*, and *Δrba1::RBA1*$^{+}$ cells to human N/TERT keratinocytes. Scale bar, 50µm. Magenta=keratinocyte; Blue=nuclei; Yellow=*C. auris.* **F)** Adherence of *C. auris* isolates and *RBA1* strains to human N/TERT keratinocytes as measured by the proportion of attached cells remaining after washing. Bars represent mean ± standard deviation for three biological replicates, statistical significance was determined using 1-way ANOVA followed by Dunnett's test

761 for multiple comparisons, *$P \leq 0.05$. **G)** Representative immunofluorescence images showing
762 adherence of *C. auris* clinical isolates harboring *RBA1*^{Q174*}, *RBA1*^{Q225*}, and *RBA1*^{C303S} mutations
763 and corresponding closest genetic relatives to human N/TERT keratinocytes. Scale bar, 50µm.
764 Magenta=keratinocyte; Blue=nuclei; Yellow=*C. auris.* Representative immunofluorescence
765 images showing adherence of SKU013 (*RBA1*^{WT}), *Δrba1*, and *Δrba1::RBA1*$^{+}$ cells to human
766 N/TERT keratinocytes. Scale bar, 50µm. Magenta=keratinocyte; Blue=nuclei; Yellow=*C. auris.* **H)**
767 Adherence of *C. auris* clinical isolates harboring *RBA1*^{Q174*}, *RBA1*^{Q225*}, and *RBA1*^{C303S} mutations
768 and corresponding closest genetic relatives to human N/TERT keratinocytes as measured by the
769 proportion of attached cells remaining after washing. Bars represent mean ± standard deviation
770 for three biological replicates, statistical significance was determined using 1-way ANOVA
771 followed by Dunnett's test for multiple comparisons, *$P \leq 0.05$.
772

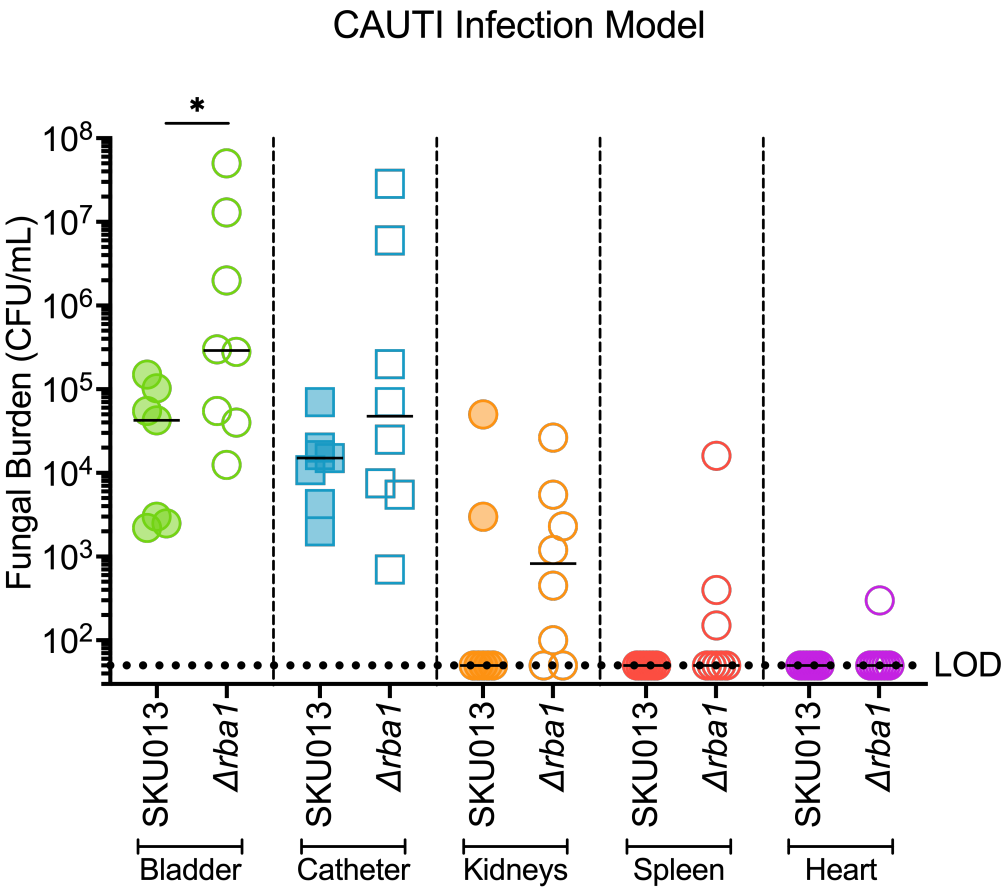

Figure 7. Loss of *RBA1* results in greater fungal burden in a murine model of catheter associated urinary tract infection. Fungal burden of SKU013 and the derivative *Δrba1* strain obtained from the catheter material or bladder, kidney, spleen, and heart tissues after infection in a murine model of catheter associated urinary tract infection (CAUTI). Two-tailed Mann-Whitney tests showed significant differences in fungal burden recovered from bladder tissue (*$P \leq 0.05$, n=8 mice per group). CFU, colony forming units; LOD, lower limit of detection.

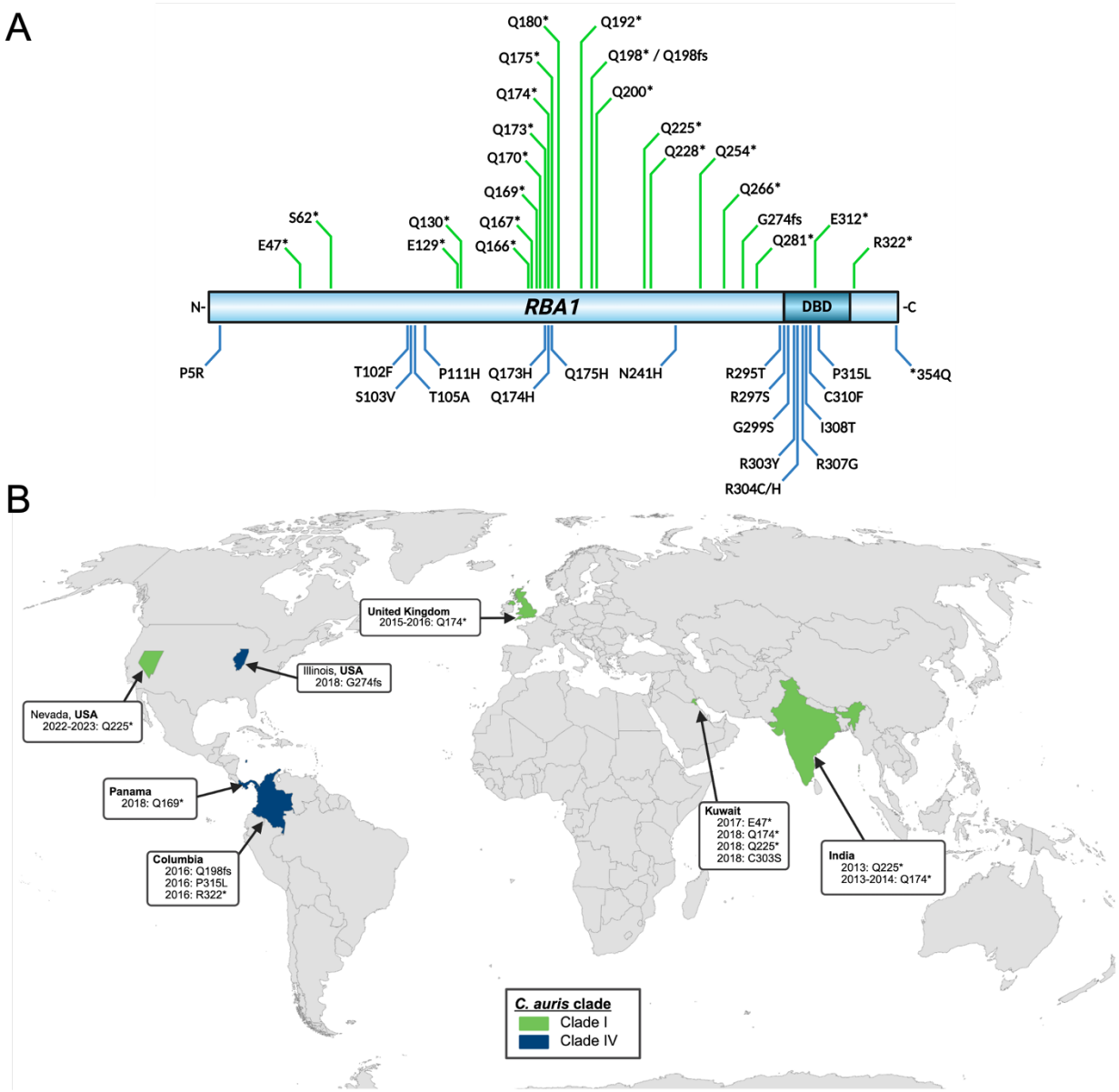

Figure 8. Identification of *RBA1* mutations emerging during numerous outbreaks of *C. auris* infections worldwide. A) Diagram depicting non-synonymous mutations in *RBA1* identified by analyzing publicly available *C. auris* whole genome sequencing data. Green lines on top of figure indicate early stop codons and frameshift mutations. Blue lines on bottom of figure indicate missense mutations. N241H and *354Q were identified among all clinical isolates classified as clade IV. DBD: DNA-binding domain. **B)** World map indicating locations of documented outbreaks of *C. auris* infections where mutations in *RBA1* were identified from publicly available data. Green fill indicates outbreaks involving isolates representing genetic Clade I and blue fill indicates outbreaks involving isolates representing genetic clade IV. *RBA1* mutations identified from publicly available sequencing of a global collection of *C. auris* isolates.

795

	Culture Source	SNPs vs SKU013	*RBA1*	Susceptibility		
				FLU	AmB	Echino
Patient 51						
SKU013	Endotracheal asp.	-	WT	**R**	S	S
SKU014	Endotracheal asp.	2	WT	**R**	S	S
SKU015	Endotracheal asp.	4	WT	**R**	S	S
SKU016	Endotracheal asp.	4	WT	**R**	S	S
SKU017	Endotracheal asp.	4	WT	**R**	S	S
SKU018	Urine	8	**E47***	**R**	S	**R**
SKU020	Blood	5	WT	**R**	S	S
Patient 53						
SKU022	Endotracheal asp.	6	**E47***	**R**	S	S
SKU023	Endotracheal asp.	6	**E47***	**R**	S	S
SKU026	Tracheal sec.	7	**E47***	**R**	S	S
SKU031	Urine	7	**E47***	**R**	**R**	S
SKU032	Urine	89	WT	**R**	S	S
SKU033	Urine	8	**E47***	**R**	**R**	S
SKU035	Urine	8	**E47***	**R**	S	**R**

796
797

798 **Table 1. Description of isolates obtained from patient cases 51 and 53.** Isolates name, culture
799 source, number of SNPs in coding regions relative to the earliest isolate SKU013, *RBA1*
800 genotype, and interpretation of susceptibility to fluconazole (FLU), amphotericin B (AmB), and
801 echinocandins (Echino) based on current CDC tentative breakpoints. SNPs: single nucleotide
802 polymorphisms.

803

804
805

REFERENCES

1. World Health Organization. *WHO fungal priority pathogens list to guide research, development and public health action*. (World Health Organization, Geneva, 2022).

2. Satoh K, Makimura K, Hasumi Y, Nishiyama Y, Uchida K, Yamaguchi H. *Candida auris* sp. nov., a novel ascomycetous yeast isolated from the external ear canal of an inpatient in a Japanese hospital. *Microbiol Immunol* **53**, 41-44 (2009).

3. Lockhart SR*, et al.* Simultaneous Emergence of Multidrug-Resistant *Candida auris* on 3 Continents Confirmed by Whole-Genome Sequencing and Epidemiological Analyses. *Clin Infect Dis* **64**, 134-140 (2017).

4. European Centre for Disease Prevention and Control. *Survey on the epidemiological situation, laboratory capacity and preparedness for Candidozyma (Candida) auris, 2024*. (Publications Office of the European Union, 2025).

5. Sabino R, Veríssimo C, Pereira Á A, Antunes F. *Candida auris*, an Agent of Hospital-Associated Outbreaks: Which Challenging Issues Do We Need to Have in Mind? *Microorganisms* **8**, (2020).

6. Baker AD, Gold JAW, Forsberg K, Jones S, Lyman MM. Progression from *Candida auris* Colonization Screening to Clinical Case Status, United States, 2016-2023. *Emerg Infect Dis* **31**, 1613-1617 (2025).

7. Gülten E*, et al. Candida auris* vs. Non-*Candida auris* Candidemia in Critically Ill Patients: Clinical Outcomes, Risk Factors, and Mortality. *J Fungi (Basel)* **11**, (2025).

8. Arslan E*, et al.* Comparison of risk factors and mortality of candidemia by *Candida auris* versus *Candida* non-*auris* in intensive care units. *Infect Dis (Lond)*, 1-15 (2025).

9. Akinbobola AB, Kean R, Hanifi SMA, Quilliam RS. Environmental reservoirs of the drug-resistant pathogenic yeast *Candida auris*. *PLoS Pathog* **19**, e1011268 (2023).

10. Proctor DM*, et al.* Clonal *Candida auris* and ESKAPE pathogens on the skin of residents of nursing homes. *Nature* **639**, 1016-1023 (2025).

11. Pacilli M*, et al.* Regional Emergence of *Candida auris* in Chicago and Lessons Learned From Intensive Follow-up at 1 Ventilator-Capable Skilled Nursing Facility. *Clin Infect Dis* **71**, e718-e725 (2020).

12. Chow NA, *et al.* Multiple introductions and subsequent transmission of multidrug-resistant *Candida auris* in the USA: a molecular epidemiological survey. *The Lancet Infectious Diseases* **18**, 1377-1384 (2018).

13. Lyman M, *et al.* Worsening Spread of *Candida auris* in the United States, 2019 to 2021. *Ann Intern Med* **176**, 489-495 (2023).

14. Lyman M, *et al.* Notes from the Field: Transmission of Pan-Resistant and Echinocandin-Resistant *Candida auris* in Health Care Facilities - Texas and the District of Columbia, January-April 2021. *MMWR Morb Mortal Wkly Rep* **70**, 1022-1023 (2021).

15. Rybak JM, *et al.* In vivo emergence of high-level resistance during treatment reveals the first identified mechanism of amphotericin B resistance in *Candida auris*. *Clin Microbiol Infect* **28**, 838-843 (2022).

16. Codda G, *et al.* In vivo evolution to echinocandin resistance and increasing clonal heterogeneity in *Candida auris* during a difficult-to-control hospital outbreak, Italy, 2019 to 2022. *Euro Surveill* **28**, (2023).

17. Carolus H, *et al.* Genome-Wide Analysis of Experimentally Evolved *Candida auris* Reveals Multiple Novel Mechanisms of Multidrug Resistance. *mBio* **12**, (2021).

18. Rybak JM, *et al.* Mutations in *TAC1B*: a Novel Genetic Determinant of Clinical Fluconazole Resistance in *Candida auris*. *mBio* **11**, (2020).

19. La Bella AA, Santiago-Tirado FH, Flores-Mireles AL. *Candida auris* is emerging as a prevalent urinary pathogen. *PLoS Pathog* **21**, e1013138 (2025).

20. Chow NA, *et al.* Tracing the Evolutionary History and Global Expansion of *Candida auris* Using Population Genomic Analyses. *mBio* **11**, (2020).

21. Muñoz JF, *et al.* Clade-specific chromosomal rearrangements and loss of subtelomeric adhesins in *Candida auris*. *Genetics* **218**, (2021).

22. Barker KS, *et al.* Relative contributions of the *ERG11*$^{(VF125AL)}$ and *MRR1A*$^{(N647T)}$ mutations to fluconazole resistance in Clade III *Candidozyma (Candida) auris* clinical isolates. *Clin Microbiol Infect*, (2025).

23. Rybak JM, Sharma C, Doorley LA, Barker KS, Palmer GE, Rogers PD. Delineation of the Direct Contribution of *Candida auris ERG11* Mutations to Clinical Triazole Resistance. *Microbiol Spectr* **9**, e0158521 (2021).

24. Mayr EM, Ramírez-Zavala B, Krüger I, Morschhäuser J. A Zinc Cluster Transcription Factor Contributes to the Intrinsic Fluconazole Resistance of *Candida auris*. *mSphere* **5**, (2020).

25. Massic L*, et al.* Acquired amphotericin B resistance attributed to a mutated *ERG3* in *Candidozyma auris*. *Antimicrob Agents Chemother* **69**, e0060125 (2025).

26. Doorley LA, Meza-Perez V, Jones SJ, Rybak JM. A *Candidozyma (Candida) auris*-Optimized Episomal Plasmid-Induced Cas9-Editing System Reveals the Direct Impact of the S639F-Encoding *FKS1* Mutation. *J Infect Dis* **232**, e529-e536 (2025).

27. Spruijtenburg B*, et al.* Whole genome sequencing analysis demonstrates therapy-induced echinocandin resistance in *Candida auris* isolates. *Mycoses* **66**, 1079-1086 (2023).

28. Asadzadeh M*, et al.* Molecular characterisation of *Candida auris* isolates from immunocompromised patients in a tertiary-care hospital in Kuwait reveals a novel mutation in *FKS1* conferring reduced susceptibility to echinocandins. *Mycoses* **65**, 331-343 (2022).

29. La Bella AA*, et al.* The catheterized bladder environment promotes Efg1- and Als1-dependent *Candida albicans* infection. *Science Advances* **9**, eade7689 (2023).

30. Zhao G*, et al.* Adhesin Als4112 promotes *Candida auris* skin colonization through interactions with keratinocytes and extracellular matrix proteins. *Nat Commun* **16**, 5673 (2025).

31. Santana DJ*, et al.* A *Candida auris*-specific adhesin, Scf1, governs surface association, colonization, and virulence. *Science* **381**, 1461-1467 (2023).

32. de Assis LJ*, et al.* Nature of β-1,3-Glucan-Exposing Features on *Candida albicans* Cell Wall and Their Modulation. *mBio* **13**, e0260522 (2022).

33. Hopke A, Nicke N, Hidu EE, Degani G, Popolo L, Wheeler RT. Neutrophil Attack Triggers Extracellular Trap-Dependent *Candida* Cell Wall Remodeling and Altered Immune Recognition. *PLoS Pathog* **12**, e1005644 (2016).

34. Yang M*, et al.* Control of β-glucan exposure by the endo-1,3-glucanase Eng1 in *Candida albicans* modulates virulence. *PLoS Pathog* **18**, e1010192 (2022).

35. Louvet M*, et al.* Ume6-dependent pathways of morphogenesis and biofilm formation in Candida auris. *Microbiol Spectr* **12**, e0153124 (2024).

36. Conover MS, Flores-Mireles AL, Hibbing ME, Dodson K, Hultgren SJ. Establishment and Characterization of UTI and CAUTI in a Mouse Model. *J Vis Exp*, e52892 (2015).

37. Escandón P*, et al.* Notes from the Field: Surveillance for *Candida auris* - Colombia, September 2016-May 2017. *MMWR Morb Mortal Wkly Rep* **67**, 459-460 (2018).

38. Barbian HJ*, et al. Candida auris* Outbreak and Epidemiologic Response in Burn Intensive Care Unit, Illinois, USA, 2021-2023. *Emerg Infect Dis* **31**, 438-447 (2025).

39. Rhodes J*, et al.* Genomic epidemiology of the UK outbreak of the emerging human fungal pathogen *Candida auris*. *Emerg Microbes Infect* **7**, 43 (2018).

40. Araúz AB*, et al.* Isolation of *Candida auris* from 9 patients in Central America: Importance of accurate diagnosis and susceptibility testing. *Mycoses* **61**, 44-47 (2018).

41. Chowdhary A*, et al.* New clonal strain of Candida auris, Delhi, India. *Emerg Infect Dis* **19**, 1670-1673 (2013).

42. Gorzalski A*, et al.* The use of whole-genome sequencing and development of bioinformatics to monitor overlapping outbreaks of Candida auris in southern Nevada. *Front Public Health* **11**, 1198189 (2023).

43. Carolus H*, et al.* Acquired amphotericin B resistance leads to fitness trade-offs that can be mitigated by compensatory evolution in *Candida auris*. *Nat Microbiol* **9**, 3304-3320 (2024).

44. Burrack LS, Todd RT, Soisangwan N, Wiederhold NP, Selmecki A. Genomic Diversity across *Candida auris* Clinical Isolates Shapes Rapid Development of Antifungal Resistance In Vitro and In Vivo. *mBio* **13**, e0084222 (2022).

45. Mishra A, Aggarwal A, Khan F. Medical Device-Associated Infections Caused by Biofilm-Forming Microbial Pathogens and Controlling Strategies. *Antibiotics (Basel)* **13**, (2024).

46. Molina JJ, Flores-Mireles AL. CAUTIon - not all UTIs are the same. *Nat Rev Urol* **22**, 799-814 (2025).

47. Ahmad S, Khan Z, Al-Sweih N, Alfouzan W, Joseph L. *Candida auris* in various hospitals across Kuwait and their susceptibility and molecular basis of resistance to antifungal drugs. *Mycoses* **63**, 104-112 (2020).

48. Gulati M*, et al.* In Vitro Culturing and Screening of *Candida albicans* Biofilms. *Curr Protoc Microbiol* **50**, e60 (2018).

49. Schindelin J*, et al.* Fiji: an open-source platform for biological-image analysis. *Nat Methods* **9**, 676-682 (2012).

50. Dickson MA*, et al.* Human keratinocytes that express hTERT and also bypass a p16(INK4a)-enforced mechanism that limits life span become immortal yet retain normal growth and differentiation characteristics. *Mol Cell Biol* **20**, 1436-1447 (2000).

51. Lamprecht MR, Sabatini DM, Carpenter AE. CellProfiler: free, versatile software for automated biological image analysis. *Biotechniques* **42**, 71-75 (2007).